

Original Article

Comparative analysis of protein profiles between wild-type and *Runx3* null mouse embryonic stem cells lines

Oh Kwang Kwon, Mu Seog Choe, You Mie Lee, Sangkyu Lee*, Min Young Lee*

College of Pharmacy, Research Institute of Pharmaceutical Sciences, Kyungpook National University, Daegu 41566, Korea

Runt related transcription factors (RUNX), a family of well-known transcription factors, play key regulatory roles in diverse biological processes, such as proliferation, differentiation, and DNA repair. Of RUNX family, RUNX3 is the least well characterized of the three family members. Nevertheless, the role of RUNX3 as a key regulator in essential biological pathways has been reported and inactivation of RUNX3 leads to a variety of disease, such as cancer, via regulation of Wnt signaling and K-ras mutations in many mammalian tissues. Recent studies using RUNX3-deficient cells and mice revealed an association with hematopoiesis and hypersensitivity to granulocyte-colony stimulating factor. Nevertheless, protein dynamics associated with RUNX3 remain poorly understood. In the present study, we performed a large-scale protein study from *Runx3* knockout (KO) mouse embryonic stem cells (mESC) using a stable isotope labeling by amino acids (SILAC)-based quantitative proteomics approach. The results showed that 67 proteins were significantly up and downregulated after *Runx3* KO. Bioinformatic analyses that revealed that these proteins have diverse biological functions, such as substances transport and cellular structure. Thus, our results enhance our current understanding of the function of RUNX3 in mESCs and suggest potential roles for RUNX proteins in diverse diseases. Additionally, our results can be used as a database to help us understand the mechanism of action of RUNX3.

Key words: related transcription factors (RUNX3), mouse embryonic stem cells, stable isotope labeling by amino acids (SILAC), quantitative proteomics, bioinformatics

Introduction

The first mammalian Runt domain transcription factor (*RUNX*) gene was cloned and its association with human disease was revealed in 1991 [1]. During the past two decades, studies have investigated the function, structural elements, genetic variants, and roles in normal development and pathological conditions of the RUNX family [2]. In mammals, there are three RUNX genes, *RUNX1*, *RUNX2*, and *RUNX3*, and RUNX proteins are well conserved among many different species.

RUNX3 is the least well characterized of the three family members. Nevertheless, the role of RUNX3 as a key regulator in essential biological pathways has been reported. Diverse *RUNX3*-deficiency models have shown that inactivation of *RUNX3*, as tumor suppressor, promotes tumorigenesis in many tissues. The loss of *RUNX3* expression is causally linked to the genesis of human gastric cancer [3]. *RUNX3* inactivation independently induced intestinal adenomas by attenuating Wnt signaling, and lung adenomas via *K-RAS* mutations [4, 5]. Moreover, RUNX3 is a key regulator in the response of hypoxia and immune cell infiltration into the tumor microenvironment [6]. In mice, the conditional knockout (KO) of *Runx3* resulted in the mice developing a myeloproliferative disorder, and *RUNX3*-deficient cells showed hypersensitivity to granulocyte-colony stimulating factor [7]. In our model, *Runx3* null mice die soon after birth, often from starvation, because of multiple gastrointestinal organ defects, such as hypertrophic intestinal and stomach walls [3, 8, 9], although other organ defects have been reported. Although the functions of RUNX3 have been reported in diverse *RUNX3*-deficient models, the protein expression

*Corresponding author: Min Young Lee

College of Pharmacy, Research Institute of Pharmaceutical Sciences, Kyungpook National University, Daegu 41566, Korea
Tel: +82-53-950-8577, Fax: +82-53-950-8557, E-mail: vetmedic@knu.ac.kr
Sangkyu Lee

College of Pharmacy, Research Institute of Pharmaceutical Sciences, Kyungpook National University, Daegu 41566, Korea
Tel: +82-53-950-8571, Fax: +82-53-950-8557, E-mail: sangkyu@knu.ac.kr

fingerprint associated with *RUNX3* deficiency, which would provide clues to *RUNX3*-related molecular mechanisms, is incompletely understood. Additionally, to analyze phenotypes at the adult stage is difficult using our model, because *Runx3* null mice show early lethality; however, it is possible to study the cellular profiles of *RUNX3* in early developmental stages by establishing a *Runx3* null mouse embryonic stem cell (mESC) line. Thus, in the present study, we measured the dynamics of protein expression in *Runx3* KO mESCs based on comparative quantified proteomics coupled with a stable isotope labeling by amino acids (SILAC) based-metabolic labeling system.

Materials and Methods

Establishment and maintenance of a *Runx3* KO mESC line

To generate a *Runx3* KO mESC line, male and female *Runx3* heterozygous (+/-) mice were mated. On day 3.5 of pregnancy, the female mouse was sacrificed and the blastocysts were flushed from the uterine horns using M2 medium (Sigma-Aldrich, St. Louis, MO, USA). After washing with M2 medium, the zona pellucida was removed using acidic Tyrode's Solution (Sigma-Aldrich). After washing, the blastocysts were plated onto a mouse embryonic fibroblast (MEF) feeder layer. After 7 days, the inner cell mass (ICM) outgrowth was physically removed from the surrounding trophoblast cells and transferred to a drop of Accutase (Sigma-Aldrich) and incubated at 37°C for 20 min. ICM outgrowths were dissociated into small cell clumps of 5–10 cells using mechanical force with P200 pipette. The cell clumps from each ICM outgrowth were transferred into separate wells of a MEF-plated 12-well plate containing mESC culture medium [Dulbecco's modified Eagle's medium (DMEM; Invitrogen) supplemented with 1% penicillin and streptomycin (Invitrogen), 2 mM L-glutamine (Invitrogen), 0.1 mM non-essential amino acid (MEM-NEAA; Invitrogen), 1 mM sodium pyruvate (Invitrogen), 0.1 mM 2-mercaptoethanol (Sigma), 10 µg/mL leukemia inhibitory factor (LIF), and 15% knock-out serum replacement (KO-SR; Invitrogen)] supplemented 10 µM Y-27632 (a selective p160ROCK inhibitor) for 4 days. mESCs were maintained and subcultured every 3–4 days in mESC medium without Y-27632. To deplete the feeder cells, mESC colonies of each line were manually picked up and dissociated into single cells using 0.25% trypsin-EDTA (Invitrogen). Dissociated cells were plated on 0.2% gelatin-coated culture dishes containing mESC culture medium supplemented with 20 µg/mL LIF. After expansion and feeder depletion of the mESCs, the presence or absence of the wild-type gene was confirmed using genomic DNA PCR analysis (Fig. 1A and

1B).

SILAC of *RUNX3* KO embryonic stem cells

Feeder-depleted *Runx3* wild-type cells (light control) were grown in DMEM without isotopes and supplemented with 1% penicillin and streptomycin, 2 mM L-glutamine, 0.1 mM non-essential amino acid, 1 mM sodium pyruvate, 0.1 mM 2-mercaptoethanol, 20 µg/mL LIF, and 15% KO-SR. In addition, Feeder-depleted *Runx3* KO mESCs were labeled with heavy amino acids by five passages of growth in SILAC medium comprising DMEM with 100 mg/L L-lysine-¹³C₆-¹⁵N₂ and 100 mg/L L-arginine-¹³C₆-¹⁵N⁴ (Cambridge Isotope Laboratories, Andover, MA, USA) supplemented with 1% penicillin and streptomycin, 2 mM L-glutamine, 0.1 mM non-essential amino acid, 1 mM sodium pyruvate, 0.1 mM 2-mercaptoethanol, 20 µg/mL LIF, and 15% KO-SR. The labeling efficiency of heavy lysine and arginine was at least 95% (data not shown).

Cell lysis and in-solution digestion

The SILAC-treated cells were lysed using radioimmuno-precipitation assay (RIPA) buffer (25 mM Tris-HCl pH 7.6, 150 mM NaCl, 1% NP-40, 1% sodium deoxycholate, 0.1% SDS) and sonication for 5 sec (six times) on ice. Extracted proteins were precisely measured using a BCA protein assay kit (Thermo Fisher scientific, Waltham, MA, USA). For the SILAC experiments, proteins from heavy labeled *Runx3* (-/-) and un-labeled (light) wild-type were combined in equal amounts. To carry out reduction and alkylation, samples were incubated with 15 mM DL-dithiothreitol (DTT) at 57°C for 30 min. Then, 60 mM iodoacetamide (IAA) was added to proteins and incubated for 30 min in dark. Four volumes of ice-cold acetone was then added to the proteins to remove the detergent and incubated for 4 h at -20°C. After centrifugation at 14,000×g for 10 min at 4°C, the supernatant was discarded and the pellet was washed twice with ice-cold acetone. The purified proteins were resuspended in 100 mM Triethylammonium bicarbonate (TEAB) buffer and subjected to trypsin digestion at 37°C for 16 h. Peptides were dried using a speed vacuum system and dissolved in water with 0.1% formic acid. To separate the peptides, a High pH Reversed-Phase Peptide Fractionation Kit (Thermo Fisher Scientific) was used according to the manufacturer's protocol.

In addition to increasing number of proteins for the deep proteomics approach, we applied in-gel digestion as another fractionation step, following a method detailed in a previous publication [10]. Briefly, we performed SDS-PAGE with mixed proteins and then stained the gel using colloidal Coomassie blue staining solution (National Diagnostics, Atlanta, GA, USA). We divided the gel into

seven equal pieces, which were reduced and alkylated using DTT and IAA, respectively. Finally, the gel pieces were digested by trypsin at 37°C overnight. Peptides extracted from gel were dried using the speed vacuum system. Total fractionated samples were desalted using a C18 Ziptip and dried completely using the speed vacuum system.

Instruments for quantitative proteomics

The digested peptides were dissolved in solution A (2% acetonitrile in 0.1% formic acid). We then analyzed the samples using a high resolution Q-Exactive Hybrid Quadrupole-Orbitrap™ Mass Spectrometer (Thermo Fisher Scientific) connected with an EASY-nLC 1000 liquid chromatography system (Thermo Fisher Scientific). The samples were loaded into a homemade C12 column (Proteo C12 4 μm beads, 90-Å pore size, Phenomenex, Torrance, CA, USA) and separated using 2%–24% solution B (100% Acetonitrile with 0.1% formic acid) for 45 min and then with 24%–90% solution B for 15 min at 200 nL/min. Mass spectrometry (MS) data were acquired using following parameters: A scan range of 300 to 1,400 m/z, using a lock mass at 445.12002 (+); for full MS, 70,000 resolution, 3e6 AGC target, and 50 ms maximum IT, as well as 25 sec dynamic exclusion; for the MS/MS spectra, 17,500 resolution, 1e5 AGC target, 75 ms maximum IT, and the top 15 data-dependent mode with 27 NCE.

Protein annotation and bioinformatic analysis

Protein annotation

MS data were analyzed using MaxQuant 1.4.1.2 against the UniProt mouse database (with includes 51,444 protein sequences) to identify and quantify the proteins [11]. The search parameters were as follows: Trypsin as the enzyme was applied with two missed cleavages; mass tolerances of 7 ppm and 20 ppm for fragment mass deviation; Carbamidomethyl at Cys (57.021 Da) as a fixed modification; however, oxidation at Met (15.995 Da) and protein N-terminal acetylation (42.011 Da) were set as variable modifications. For the SILAC quantified ratio, heavy labeled means ¹³C₆-¹⁵N₂ labeled lysine (8.014 Da), and ¹³C₆-¹⁵N₄ labeled arginine (10.008 Da). All pair-wise protein ratios were calculated between *Runx3* KO vs. control with a minimum ratio count of two. All other parameters in MaxQuant were set to default values. To select potential unique proteins, identified proteins were filtered for a false discovery rate (FDR) less than 1%, and contaminants and those only represents by 1 peptide/protein were removed. Also, visualization using a scatter plot and the calculation of the Pearson correlation were performed using Perseus 1.6.

Bioinformatic analyses

Analysis of Gene Ontology (GO) and InterPro enrichment were performed on the up and downregulated proteins via the web-based algorithm, David 6.8, according to a previously described procedure [12]. Furthermore, we conducted protein-protein interaction analysis of the differentially expressed proteins (DEPs) using STRING 10.5 [13]. The default parameters in David and STRING were used.

Results and Discussion

SILAC of *Runx3* KO embryonic stem cells

To investigate the changed protein profile induced by *Runx3* KO in mESCs, we established *Runx3* KO mESC lines (Fig. 1A and 1B). We cultured the mESCs in the presence of light (Lys-0 and Arg-0) wild-type (WT) cells or heavy lysine (Lys-8) and arginine (Arg-10) for KO cells for SILAC-based quantitative proteomic analysis (Fig. 1C). The SILAC cell lysates were mixed in equal amounts and digested into peptides using trypsin. After fractionation of the tryptic peptides using high pH reversed-phase peptide fractionation, the protein level was assessed using nano-LC-MS/MS using a hybrid Quadrupole-Orbitrap™ mass spectrometer. Moreover, we applied in-gel digestion as additional fractionation approach to increase the number of quantified proteins for deep proteomics approach. The obtained MS/MS spectra were analyzed using MaxQuant software. In total, 3,537 proteins were identified, of which 3,492 (98.7%) were quantifiable with a protein-level FDR < 0.01 (Fig. 1D). The 3,537 proteins are listed in Supplementary Table S1.

Among the 3,492 quantified proteins, 29 proteins were upregulated (normalized Heavy / Light (H/L) ratio > 2.0) and 38 proteins were downregulated (normalized H/L ratio < 0.5) in the *Runx3* KO mESCs (Fig. 1D). The DEPs are summarized in Tables 1 and 2 for upregulated and downregulated proteins, respectively. The most upregulated proteins were ATP-dependent (S)-NAD(P)H-hydrate dehydratase (H/L ratio 8.4) and peroxisomal acyl-coenzyme A oxidase 1 (H/L ratio 7.9). By contrast, serum albumin (H/L ratio 0.038) and titin (H/L ratio 0.067) were identified as the most downregulated proteins. Additionally, we used technical replicates to improve the accuracy of the results. To evaluate the reproducibility of the data, the correlation factor between the duplicated analyzed results obtained by in-gel and in sol-digestion, respectively, was calculated, which showed a significant correlation, with an R value of 0.7 or higher (Fig. 2).

Bioinformatic analysis of DEPs in *Runx3* KO cells

To further understand the protein dynamics resulting

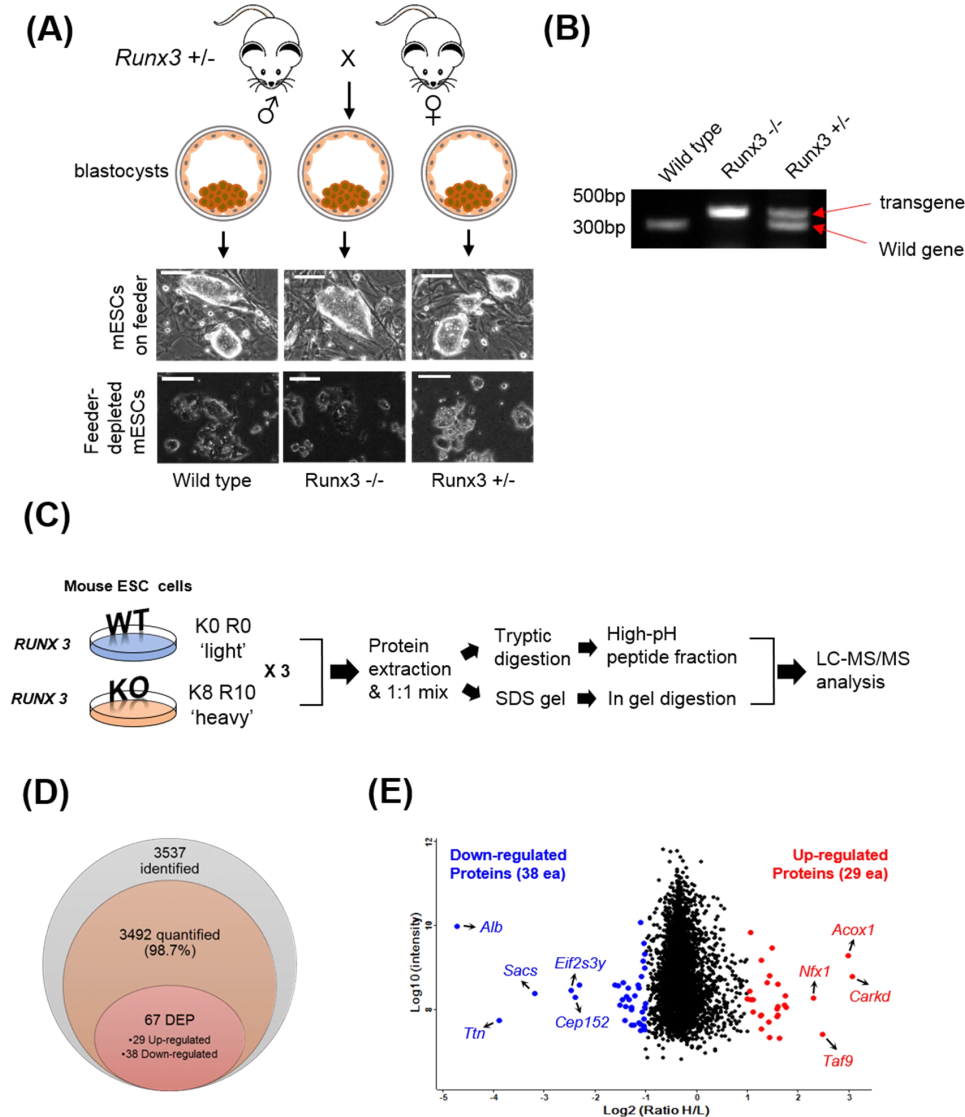


Fig. 1. Comparative proteomics in *Runx3* knockout (KO) mouse embryonic stem cells (mESCs). (A) Strategy used to establishment of *Runx3* KO mESC lines. (B) PCR-based genotyping result in *Runx3* KO mESC lines. (C) Workflow of the experimental design to evaluate and quantify proteins between *Runx3* wild-type (WT) and KO mESCs. (D) Venn diagram representing to total protein identification. (E) Scatter plot and distribution of differentially expressed proteins (DEPs) between *Runx3* WT vs. KO.

from loss of *Runx3* in mESCs, we performed GO term enrichment analyses for the DEPs using the DAVID software (Fig. 3A). Generally, the enrichment of GO terms in the upregulated DEPs was distinct from enrichment in the downregulated DEPs. In the GO biological pathway (GOBP) category, the upregulated DEPs in *Runx3* KO mESCs were associated with receptor-mediated endocytosis, hemoglobin import, and cobalamin transport, represented by proteins such as cubilin and amnionless. By contrast, the downregulated DEPs were enriched in diverse biological pathways, such as hemolysis, amino acid

biosynthetic process, and reactive oxygen regulation.

The GO cellular component (GOCC) category was also clearly distinguished between the upregulated and downregulated DEPs in the *Runx3* KO mESCs. In GOCC, the upregulated DEPs were linked to substances transfer into cells, such as clathrin-coated pits, endocytic vesicles, and membranes. Whereas the downregulated DEPs in the GOCC category were associated with diverse cell components. Even in the GO molecular function (GOMF) category, the upregulated DEPs were enriched in material transport, such as symporter activity. The downregulated

Table 1. Upregulated differentially expressed proteins in *Runx3* KO mESCs

Accession	Protein name	Gene name	Sequence coverage [%]	KO/WT ratio
J3QN06	ATP-dependent (S)-NAD(P)H-hydrate dehydratase	Carkd	11	8.4
A2A848	Peroxisomal acyl-coenzyme A oxidase 1	Acox1	4.3	7.9
A0A087WRI5	Adenylate kinase isoenzyme 6	Taf9	58.5	5.6
B1AY10	Transcriptional repressor NF-X1	Nfx1	2.8	4.9
P26618	Platelet-derived growth factor receptor alpha	Pdgfra	2.6	3.4
Q3V3K3	Serine/threonine-protein kinase TAO3	Taok3	6.6	3.4
Q8BXQ2	GPI transamidase component PIG-T	Pigt	4.3	3.3
O35709	Ectoderm-neural cortex protein 1	Enc1	4.2	3.1
D3Z2Q7	Hemicentin-1	Hmcn1	0.3	3.0
Q3TLX9	Acid sphingomyelinase-like phosphodiesterase 3b	Smpdl3b	16.4	3.0
Q8CFE6	Sodium-coupled neutral amino acid transporter 2	Slc38a2	5.8	3.0
Q6PFV6	Ephrin type-A receptor 5	Epha5	2.9	3.0
Q3UDP9	Monocarboxylate transporter 4	Slc16a3	7.2	3.0
Q9JLB4	Cubilin	Cubn	19.1	2.8
A2ARV4	Low-density lipoprotein receptor-related protein 2	Lrp2	7.2	2.7
Q99JB7	Protein amnionless	Amn	4.8	2.7
Q9Z1K8	Y+L amino acid transporter 1	Slc7a7	6.7	2.7
P11260	Putative transposase element L1Md-A101/L1Md-A102/L1Md-A2		10.9	2.6
Q3UKA4	Alcohol dehydrogenase 1	Adh1	4.5	2.4
Q99L27	GMP reductase 2	Gmpr2	9.5	2.4
E9PX84	Disabled homolog 2	Dab2	29.6	2.4
A2A5R2	Brefeldin A-inhibited guanine nucleotide-exchange protein 2	Arfgef2	1.7	2.4
D3YYG8	Redox-regulatory protein FAM213A	Fam213a	15.4	2.2
Q61609	Sodium-dependent phosphate transporter 1	Slc20a1	2.8	2.2
Q921N7	Transmembrane protein 70, mitochondrial	Tmem70	7.9	2.2
Q8K3F7	L-threonine 3-dehydrogenase, mitochondrial	Tdh	37	2.1
P15331	Peripherin	Prph	4.8	2.1
H3BLI9	TSC22 domain family protein 1	Tsc22d1	31.4	2.1
P02463	Collagen alpha-1(IV) chain	Col4a1	2.3	2.0

KO, knockout; mESC, mouse embryonic stem cells; KO/WT, knockout to wild-type ratio.

DEPs in the GOMF category notably were associated with the cytoskeleton, which was corroborated by the InterPro enrichment analysis, which indicated the predicted domains and important sites (Fig. 3B). Downregulated DEPs were associated with Tubulin functions in the InterPro

category, and the domain enrichment analysis also showed that enriched tubulin function. The upregulated DEPs were enriched in epidermal growth factor (EGF) functions in both the InterPro and domain enrichment analyses.

Fig. 4 shows the results of the protein-protein interac-

Table 2. Downregulated differentially expressed proteins in *Runx3* KO mESCs

Accession	Protein name	Gene name	Sequence coverage [%]	KO/WT ratio
Q546G4	Serum albumin	Alb	6.2	0.038
E9Q8N1	Titin	Ttn	0.1	0.067
Q9JLC8	Sacsin	Sacs	0.3	0.11
Q9Z0N2	Eukaryotic translation initiation factor 2 subunit 3, Y-linked	Eif2s3y	5.7	0.18
A2AUM9	Centrosomal protein of 152 kDa	Cep152	1.2	0.19
Q80WW9	DDR GK domain-containing protein 1	Ddrgk1	18.7	0.20
Q792Z1	MCG140784	Try10	8.1	0.33
P16627	Heat shock 70 kDa protein 1-like	Hspal1	4.5	0.34
Q91ZA3	Propionyl-CoA carboxylase alpha chain, mitochondrial	Pcca	3.2	0.35
Q91X91	Nicotinate-nucleotide pyrophosphorylase	Qprt	19.1	0.36
Q5FW91	Tubulin alpha-3 chain	Tuba3a	7.1	0.37
F6WUX1	Gamma-glutamyltranspeptidase 1	Ggt1	7.2	0.38
A0A087WP24	Alpha/beta hydrolase domain-containing protein 14B	Abhd14b	24.6	0.38
Q9DCM0	Protein ETHE1, mitochondrial	Ethe1	15.7	0.39
G3UZG5	Kelch domain-containing protein 4	Klhdc4	15.4	0.39
Q9WUL7	ADP-ribosylation factor-like protein 3	Arl3	25.3	0.40
P70278	Stimulated by retinoic acid gene 8 protein	Stra8	16	0.41
Q9CQV7	Mitochondrial import inner membrane translocase subunit TIM14	Dnajc19	36.2	0.41
D6RJ50	Presenilins-associated rhomboid-like protein, mitochondrial	Parl	14	0.41
Q9WUJ8	Origin recognition complex subunit 6	Orc6	8.4	0.43
G3UVU9	Bifunctional arginine demethylase and lysyl-hydroxylase JMJD6	Jmjd6	10.7	0.43
Q9ERD7	Tubulin beta-3 chain	Tubb3	9.1	0.45
Q9CXL3	Uncharacterized protein C7orf50 homolog		32.8	0.46
A2A4P0	ATP-dependent RNA helicase DHX8	Dhx8	1.5	0.46
Q3UY34	Uncharacterized protein C12orf43 homolog	2210016L21Rik	9.8	0.46
A0A0G2JFF9	HCLS1-associated protein X-1	Hax1	14.6	0.47
Q99K85	Phosphoserine aminotransferase	Psat1	44.1	0.47
Q99JT9	1,2-dihydroxy-3-keto-5-methylthiopentene dioxygenase	Adi1	31.8	0.47
Q80W37	Snurportin-1	Snupn	5.3	0.48
P43883	Perilipin-2	Plin2	30.6	0.48
E9Q7S1	Zinc finger protein 106	Zfp106	2.3	0.49
Q9Z127	Large neutral amino acids transporter small subunit 1	Slc7a5	13.5	0.49
Q3TCH7	Cullin-4A	Cul4a	2.8	0.49
Q9CYN9	Renin receptor	Atp6ap2	4.6	0.49
Q9ESW8	Pyroglutamyl-peptidase 1	Pgpep1	13.4	0.49
Q9DB34	Charged multivesicular body protein 2a	Chmp2a	28.4	0.50
Q922H2	[Pyruvate dehydrogenase [lipoamide]] kinase isozyme 3, mitochondrial	Pdk3	6.5	0.50
Q923D2	Flavin reductase (NADPH)	Blvrb	37.4	0.50

KO, knockout; mESC, mouse embryonic stem cells; KO/WT, knockout to wild-type ratio.

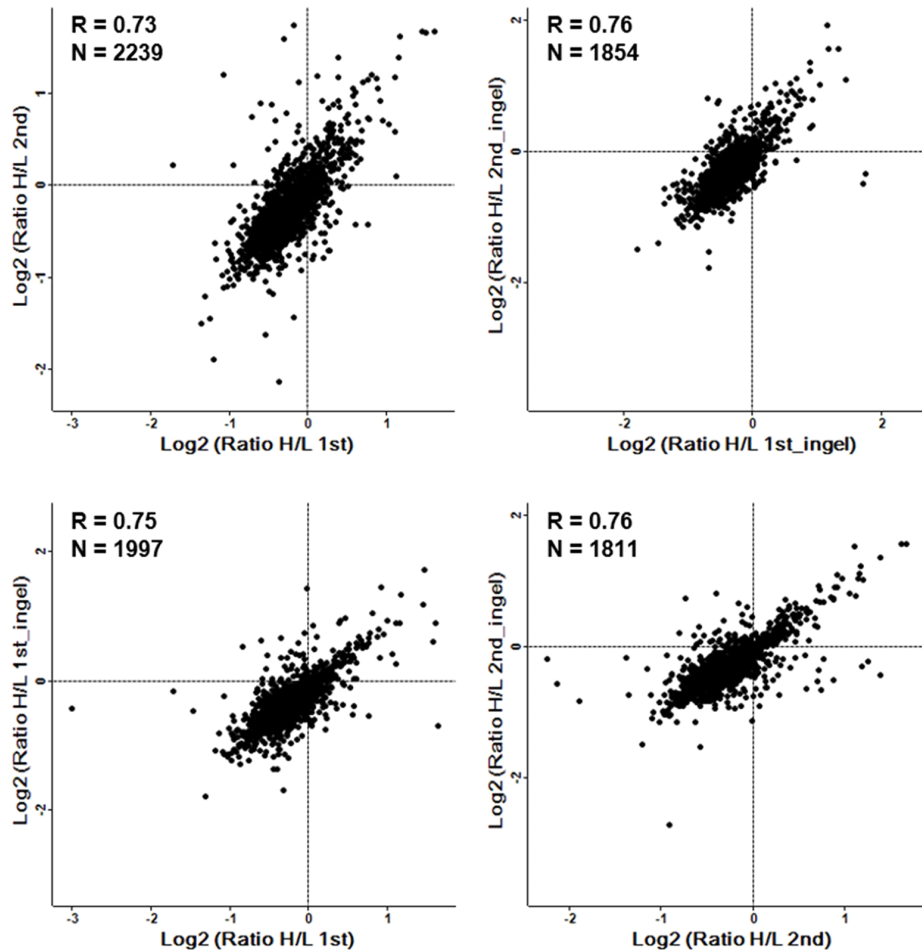


Fig. 2. Correlation plot of proteins intensities from in solution digestion and in gel digestion. The Pearson correlation coefficient is provided in each plot.

tion analysis using STRING, a search tool for recurring instances of neighboring genes among up- and downregulated DEPs, which reconstructed a network model for the DEPs [14]. In the STRING analysis of the upregulated DEPs, low-density lipoprotein receptor-related protein 2 (*Lrp2*), cubilin (*Cubn*), and protein amnionless (*Amn*) were annotated in the same cluster, which are associated with receptor-mediated endocytosis, hemoglobin import, and cobalamin transport in the GOBP category. Another cluster included peroxisomal acyl-coenzyme A oxidase 1 (*Acox1*) and L-threonine 3-dehydrogenase (*Tdh*). For the downregulated DEPs, two tubulins (*Tubb3* and *Tuba3a*) were in the main cluster in the STRING analysis (Fig. 4B). These are tubulins are linked to serum albumin (*Alb*), the most downregulated DEP, and to Heat shock 70 kDa protein 1-like (*Hspa1l*), mitochondrial import inner membrane translocase subunit TIM14 (*Dnajc19*), and ATP-dependent RNA helicase DHX8 (*Dhx8*).

Interpretation of protein profiling results in *Runx3*-deficient mESCs

In previous studies, it was reported that *Runx3* KO is related to the development of myeloproliferative disorders, like leukemogenesis, myeloid-dominant leukocytosis, and splenomegaly [7, 15, 16]. Chronic myeloproliferative disorders are a group of slow-growing blood cancers in which the bone marrow makes too many abnormal red blood cells, white blood cells, or platelets, which then accumulate in the blood. Our data suggested a mechanism by which myeloproliferative disorders occur in conditions of *RUNX3* deficiency. In *Runx3* KO mESCs, levels of proteins involved in hemoglobin import and cobalamin transport were upregulated, whereas the levels of proteins related to hemolysis of symbionts of host erythrocytes were decreased (Fig. 3). Taken together, these findings enhance our current understanding of the link between lack of the *RUNX3* protein and myeloprolifera-

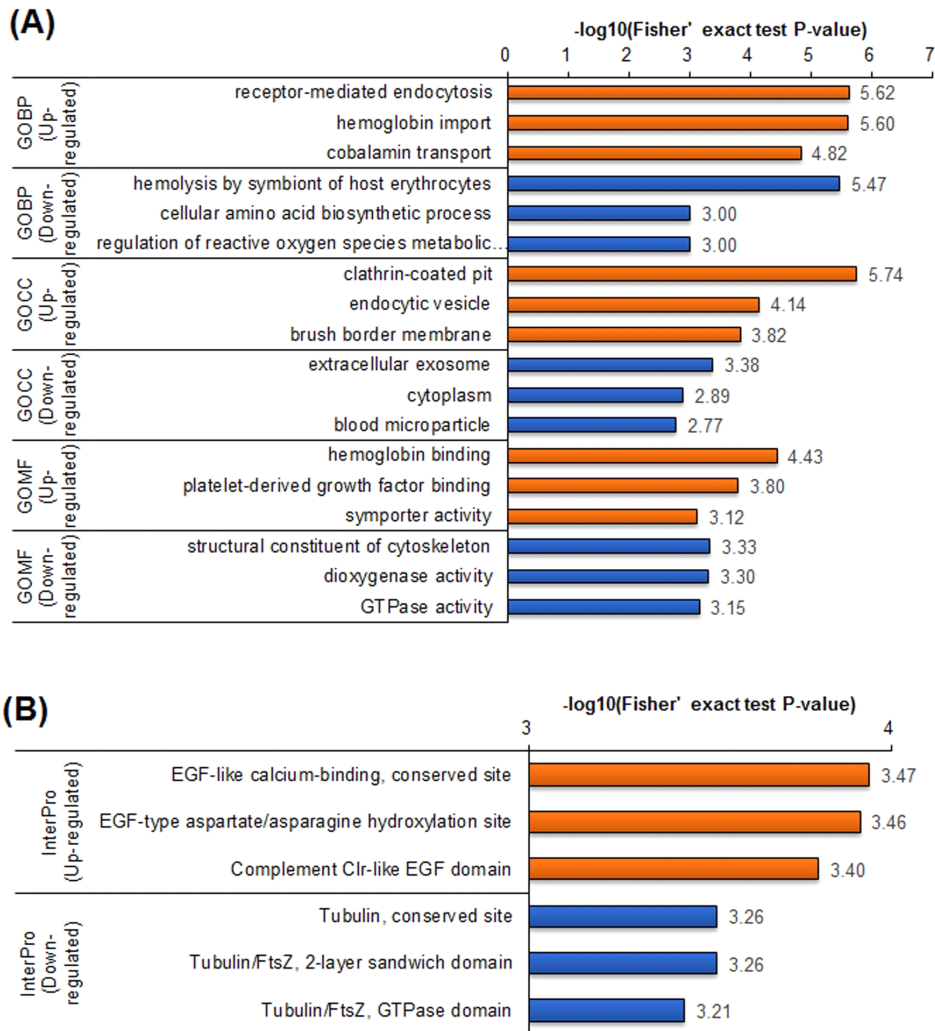


Fig. 3. Bioinformatic analysis for differentially expressed proteins (DEPs) using DAVID. gene ontology (GO) enrichment analysis (A) and InterPro (B) analysis. GOBP, GO biological pathway; GOCC, GO cellular component; GOMF, GO molecular function.

tive disorders.

In addition, the levels of tubulin alpha-3 and beta-3 chains were strongly decreased in *Runx3* KO mESCs, in which the decrease in tubulin levels were annotated in the enrichment analysis of GOMF, InterPro, and domain. In a study to find binding partners of RUNX3 using a mass spectrometry-based approach coupled with SILAC technology, RUNX3 was shown to bind to gamma-tubulin [17]. In addition, endogenous RUNX2 associates with stabilized microtubules in a concentration-dependent manner and the RUNX2 amino terminus mediates the microtubule association [18]. Moreover, RUNX3 appears to be involved in protein expression related to cell structure. Not only tubulins, but also titin, a filamentous protein spanning the half-sarcomere, was downregulated in *Runx3* KO mESCs (Table 2).

In the protein-protein interaction analysis, three proteins, low-density lipoprotein receptor-related protein 2, cubilin, and amnionless were organized in a group. These proteins are commonly associated with receptor-mediated endocytosis, hemoglobin import, and cobalamin transport in the GOBP category (Fig. 3A). In particular, mammalian cubilin and amnionless are two major receptors for protein reabsorption in the proximal tubule [19]. Cubilin was first identified as the intrinsic factor-vitamin B₁₂ receptor in mammals, and binds to albumin for renal proximal tubule protein reabsorption [20, 21]. In addition, cubilin is also involved in the renal clearance of hemoglobin [22]. Cubilin is also associated with hemoglobin binding in the GOMF category (Fig. 3A). Moreover, amnionless forms a functional receptor complex with cubilin, which is required for the endocytic function of cubilin in renal

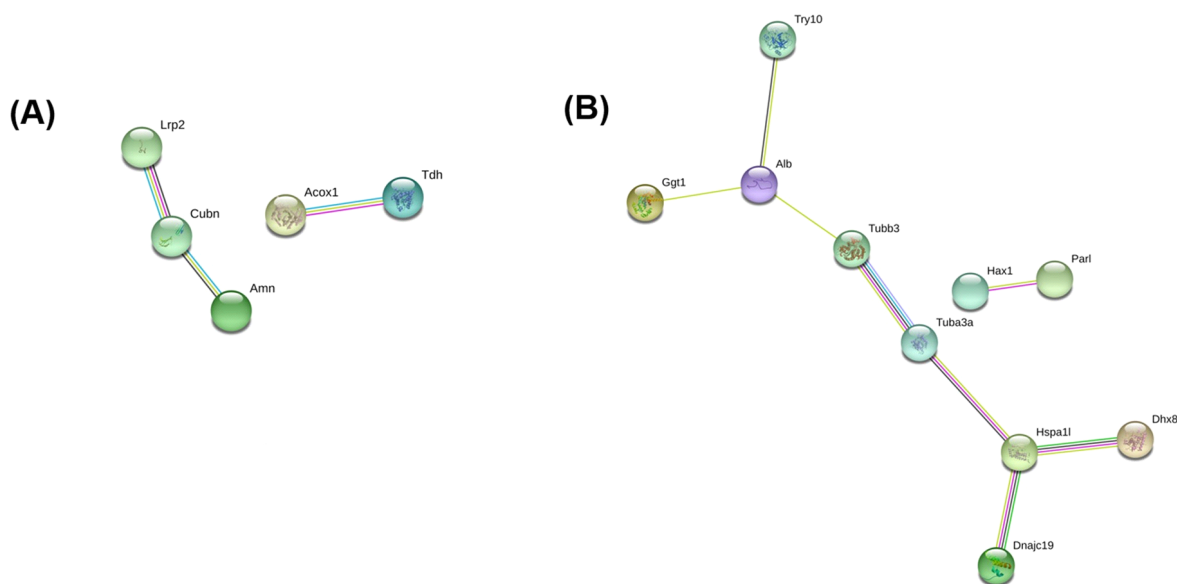


Fig. 4. Protein-protein interaction networks produced using STRING for upregulated (A) and downregulated (B) proteins (in *Runx3* knockout [KO]/wild-type [WT]).

proximal tubules [23]. Based on these observations and the results of the present study, cubilin and amnionless could be an important protein regulated by *RUNX3*.

In the present study, we investigated the protein profile in response to *Runx3* KO in mESCs using a SILAC-based quantitative proteomic strategy. We identified 3,538 proteins, and of which 3,494 proteins could be quantified. Based on GO, Interpro, and STRING analysis, significant biological processes involving *RUNX3* were suggested, especially those related to substances transport and cellular structure. Taken together, the results enhance our current understanding of the function of *RUNX3* in mESCs and suggest potential roles for *RUNX* proteins in diverse diseases.

Supplementary Materials

Supplementary materials are only available online from: <https://doi.org/10.12729/jbtr.2020.21.3.109>

Conflict of Interest

The authors declare no potential conflict of interest.

Acknowledgements

This work was supported by National Research Foundation of Korea (NRF) grants, funded by the Korean government (NRF-2012R1A4A1028835 and NRF-2018R1D1A1A02044017).

ORCID

Oh Kwang Kwon, <https://orcid.org/0000-0001-7051-2851>
 Mu Seog Choe, <https://orcid.org/0000-0002-4826-895X>
 You Mie Lee, <https://orcid.org/0000-0002-5756-7169>
 Sangkyu Lee, <https://orcid.org/0000-0001-5343-701X>
 Min Young Lee, <https://orcid.org/0000-0003-0067-2803>

Ethics Approval

This article does not require IRB/IACUC approval because there are no human and animal participants.

References

- Miyoshi H, Shimizu K, Kozu T, Maseki N, Kaneko Y, Ohki M. t(8;21) breakpoints on chromosome 21 in acute myeloid leukemia are clustered within a limited region of a single gene, AML1. *Proc Natl Acad Sci USA* 1991;88:10431-10434.
- Lee SH, Manandhar S, Lee YM. Roles of *RUNX* in hypoxia-induced responses and angiogenesis. *Adv Exp Med Biol* 2017;962:449-469.
- Li QL, Ito K, Sakakura C, Fukamachi H, Inoue K, Chi XZ, Lee KY, Nomura S, Lee CW, Han SB, Kim HM, Kim WJ, Yamamoto H, Yamashita N, Yano T, Ikeda T, Itoharu S, Inazawa J, Abe T, Hagiwara A, Yamagishi H, Ooe A, Kaneda A, Sugimura T, Ushijima T, Bae SC, Ito Y. Causal relationship between the loss of *RUNX3* expression and gastric cancer. *Cell* 2002;109:113-124.
- Ito K, Lim AC, Salto-Tellez M, Motoda L, Osato M, Chuang

- LS, Lee CW, Voon DC, Koo JK, Wang H, Fukamachi H, Ito Y. RUNX3 attenuates β -catenin/T cell factors in intestinal tumorigenesis. *Cancer Cell* 2008;14:226-237.
5. Lee YS, Lee JW, Jang JW, Chi XZ, Kim JH, Li YH, Kim MK, Kim DM, Choi BS, Kim EG, Chung JH, Lee OJ, Lee YM, Suh JW, Chuang LS, Ito Y, Bae SC. Runx3 inactivation is a crucial early event in the development of lung adenocarcinoma. *Cancer Cell* 2013;24:603-616.
 6. Manandhar S, Lee YM. Emerging role of RUNX3 in the regulation of tumor microenvironment. *BMB Rep* 2018;51:174-181.
 7. Wang CQ, Motoda L, Satake M, Ito Y, Taniuchi I, Tergaonkar V, Osato M. Runx3 deficiency results in myeloproliferative disorder in aged mice. *Blood* 2013;122:562-566.
 8. Brenner O, Levanon D, Negreanu V, Golubkov O, Fainaru O, Woolf E, Groner Y. Loss of Runx3 function in leukocytes is associated with spontaneously developed colitis and gastric mucosal hyperplasia. *Proc Natl Acad Sci USA* 2004;101:16016-16021.
 9. Lee JM, Shin JO, Cho KW, Hosoya A, Cho SW, Lee YS, Ryoo HM, Bae SC, Jung HS. Runx3 is a crucial regulator of alveolar differentiation and lung tumorigenesis in mice. *Differentiation* 2011;81:261-268.
 10. Shevchenko A, Tomas H, Havlis J, Olsen JV, Mann M. In-gel digestion for mass spectrometric characterization of proteins and proteomes. *Nat Protoc* 2006;1:2856-2860.
 11. Tyanova S, Temu T, Carlson A, Sinitcyn P, Mann M, Cox J. Visualization of LC-MS/MS proteomics data in MaxQuant. *Proteomics* 2015;15:1453-1456.
 12. Huang DW, Sherman BT, Lempicki RA. Systematic and integrative analysis of large gene lists using DAVID bioinformatics resources. *Nat Protoc* 2009;4:44-57.
 13. Szklarczyk D, Morris JH, Cook H, Kuhn M, Wyder S, Simonovic M, Santos A, Doncheva NT, Roth A, Bork P, Jensen LJ, Von Mering C. The STRING database in 2017: quality-controlled protein-protein association networks, made broadly accessible. *Nucleic Acids Res* 2017;45:D362-D368.
 14. Szklarczyk D, Franceschini A, Wyder S, Forslund K, Heller D, Huerta-Cepas J, Simonovic M, Roth A, Santos A, Tsafou KP, Kuhn M, Bork P, Jensen L J, Von Mering C. STRING v10: protein-protein interaction networks, integrated over the tree of life. *Nucleic Acids Res* 2015;43:D447-D452.
 15. Wang CQ, Krishnan V, Tay LS, Chin DW, Koh CP, Chooi JY, Nah GS, Du L, Jacob B, Yamashita N, Lai SK, Tan TZ, Mori S, Taniuchi I, Tergaonkar V, Ito Y, Osato M. Disruption of Runx1 and Runx3 leads to bone marrow failure and leukemia predisposition due to transcriptional and DNA repair defects. *Cell Rep* 2014;8:767-782.
 16. Puig-Kröger A, Corbi A. RUNX3: a new player in myeloid gene expression and immune response. *J Cell Biochem* 2006;98:744-756.
 17. Chuang LSH, Lai SK, Murata-Hori M, Yamada A, Li HY, Gunaratne J, Ito Y. RUNX3 interactome reveals novel centrosomal targeting of RUNX family of transcription factors. *Cell Cycle* 2012;11:1938-47.
 18. Pockwinse SM, Rajgopal A, Young DW, Mujeeb KA, Nickerson J, Javed A, Redick S, Lian JB, Van Wijnen AJ, Stein JL, Stein GS, Doxsey SJ. Microtubule-dependent nuclear-cytoplasmic shuttling of Runx2. *J Cell Physiol* 2006;206:354-362.
 19. Zhang F, Zhao Y, Chao Y, Muir K, Han Z. Cubilin and amnionless mediate protein reabsorption in *Drosophila nephrocytes*. *J Am Soc Nephrol* 2013;24:209-216.
 20. Kozyraki R, Fyfe J, Kristiansen M, Gerdes C, Jacobsen C, Cui S, Christensen EI, Aminoff M, De La Chapelle A, Krahe R, Verroust PJ, Moestrup SK. The intrinsic factor-vitamin B12 receptor, cubilin, is a high-affinity apolipoprotein A - I receptor facilitating endocytosis of high-density lipoprotein. *Nat Med* 1999;5:656-661.
 21. Birn H, Fyfe JC, Jacobsen C, Mounier F, Verroust PJ, Orskov H, Willnow TE, Moestrup SK, Christensen EI. Cubilin is an albumin binding protein important for renal tubular albumin reabsorption. *J Clin Invest* 2000;105:1353-1361.
 22. Gburek J, Verroust PJ, Willnow TE, Fyfe JC, Nowacki W, Jacobsen C, Moestrup SK, Christensen EI. Megalin and cubilin are endocytic receptors involved in renal clearance of hemoglobin. *J Am Soc Nephrol* 2002;13:423-430.
 23. Fyfe JC, Madsen M, Hojrup P, Christensen EI, Tanner SM, De La Chapelle A, He Q, Moestrup SK. The functional cobalamin (vitamin B12)-intrinsic factor receptor is a novel complex of cubilin and amnionless. *Blood* 2004;103:1573-1579.